Journal of Electroceramics 4:S1, 121–128, 1999

TEM, XPS and SIMS Analyzes on Grain Boundary of Lanthanum Chromites

NATSUKO SAKAI[1], TATSUO TSUNODA, NATSUO FUKUMOTO, ISAO KOJIMA, KATSUHIKO YAMAJI, TERUHISA HORITA, MASAHIKO ISHIKAWA, HARUMI YOKOKAWA & MASAYUKI DOKIYA[2]

[1]*National Institute of Materials and Chemical Research (NIMC) 1-1 Higashi, Tsukuba, Ibaraki 305 Japan*

[2]*Institute of Environmental Science and Engineering, Yokohama National University, 79-7 Tokiwadai, Hodogaya-ku, Yokohama 240, Japan*

Submitted November 17, 1997; Revised June 30, 1998; Accepted July 7, 1998

Abstract. The morphological characteristics, chromium valence state, and cation transport in the vicinity of grain boundary in $La_{1-x}Ca_xCrO_3$ were investigated by using TEM/EDS, XPS and SIMS techniques. The width of grain boundary was around 1 nm where anomalous enrichment of calcium was observed. Higher valence state of chromium such as $Cr^{6+}(d^0)$ was detected in the grain boundaries whereas $Cr^{3+}(d^3)$ and $Cr^{4+}(d^2)$ were dominant in the bulk. Very fast interdiffusion of alkaline earths was observed in the $Sr^{2+} - La_{0.75}Ca_{0.25}CrO_3$ system. All observed phenomena were correlated by assuming the A-site vacancy which may be induced by the formation of Cr^{6+} at grain boundaries.

Keywords: lanthanum chromite, grain boundary, TEM, XPS, SIMS, diffusion

1. Introduction

Lanthanum chromites with alkaline earth substitution ($La_{1-x}M_xCr_{1-y}M'_yO_3$, M′ = Ca or Sr, M′ = Mg) have been intensively investigated as candidate materials for interconnects in solid oxide fuel cells (SOFCs) [1]. The material transport properties in these lanthanum chromites, for example, diffusion of oxide ions or cations, are the most important phenomena to be investigated. The diffusion of oxide ion in an interconnect plate may cause oxygen permeation without generating electricity, which may lower the efficiency of SOFC. Cation diffusion plays an important role on sintering of interconnect plate, whereas fast cation transport can result in reactions at interfaces with other cell components such as electrodes or electrolytes.

All correspondence should be sent to: Natsuko Sakai, Energy Related Materials Group, National Institute of Materials and Chemical Research (NIMC), AIST, MITI 1-1-4, Higashi, Tsukuba, Ibaraki 305-8565 JAPAN Tel. +81 298 54 4542 Fax. +81 298 54 4540. E-mail: nsakai@home.nimc.go.jp

We have revealed that sintering of $La_{1-x}Ca_xCrO_3$ in air can be enhanced by a slightly excess amount of calcium (ca. 2 mol %) [2]. The relative density up to 94% of theoretical was obtained for $La_{0.70}Ca_{0.32}CrO_3$ by sintering at $T = 1573$ K in air, whereas the density of $La_{0.70}Ca_{0.30}CrO_3$ (no calcium excess) was only 60% of theoretial density in the same sintering condition. This is due to the formation of calcium oxychromate, $Ca_m(CrO_4)_n (m > n)$, which may exist as liquid phase between the $La_{1-x}Ca_xCrO_3$ grains at higher temperatures than their incongruent melting temperatures, and result in rapid grain growth and pore elimination [3]. Calcium enrichment was actually detected by the Auger electron spectroscopy (AES) in the vicinity (ca. 5 nm) of the fractured surface of the $La_{0.70}Ca_{0.32}CrO_3$ polycrystalline which was sintered at $T = 1573$ K and fractured along grain boundaries. It indicates that the $Ca_m(CrO_4)_n (m > n)$ reacted with $La_{1-x}Ca_xCrO_3$ at grain boundary during the sintering temperature, and as a result, the excess calcium component existed as CaO at triple junctions and a trace amount of excess calcium remained along grain boundaries.

When a sintered $La_{1-x}Ca_xCrO_3$ polycrystalline was polished and placed under an SOFC operation condition ($T = 1273\,K$, $p(O_2)$ gradient : $10^4 \sim 10^{-13}$ Pa), $Ca_m(CrO_4)_n$ appeared again on the surfaces at air side, which may result in the undesirable interface reaction with electrodes or electrolytes [4]. At the fuel side, the similar materials were supposed to appear because their decomposed compounds such as CaO and $CaCr_2O_4$ were observed. This $Ca_m(CrO_4)_n$ seems to originate from CaO at the triple junctions and migrate via grain boundaries; however, the detailed formation and transport mechanism are still remained unclear.

Such macroscopic observations indicate that the material transport via grain boundary is much faster than that via bulk, and it is closely related to the compositional distribution along grain boundaries. It must be clarified both qualitatively and quantitatively for utilization of this material during a long operation time. However, there are few investigations on the characteristics of grain boundaries of $La_{1-x}Ca_xCrO_3$. In this paper, the morphology of grain boundaries and compositional distribution were analyzed by using an transmission electron microscope/energy dispersed
X-ray analysis (TEM/EDS). The determination of valence state of chromium in the vicinity of grain boundary was made by using an X-ray photoelectron spectroscopy (XPS). The observed results are correlated with the experimental observations concerning the fast cation interdiffusion in $Sr - La_{0.75}Ca_{0.25}CrO_3$ by using a secondary ion mass spectrometry (SIMS).

2. Sample Preparation

All calcium substituted lanthanum chromites, $La_{1-x}Ca_xCrO_3$ was prepared by a liquid mixing method using aqueous solutions of metal nitrates and citric acid as starting materials, which was first reported by Pechini et al. [5] and modified in our previous papers [3]. Four compositions were selected, $La_{0.75}Ca_{0.25}CrO_3$, $La_{0.90}Ca_{0.12}CrO_3$, $La_{0.80}Ca_{0.22}CrO_3$, and $La_{0.70}Ca_{0.32}CrO_3$. A slight amount (2 mol %) of calcium excess was adopted in the latter three compositions to obtain high sinterability in air according to our previous paper [2]. The mixture of metal nitrate solutions and citric acid was heated on a hot plate to remove solvents and to form glassy gel. The gel was crashed and calcined at $T = 1173 \sim 1373\,K$ in air. The calcined powder was shaped into pellets and sintered at $T = 1573 \sim 1773\,K$ for 10 h in air. The relative densities of the sintered pellets were around $94 \sim 99\%$ of theoretical density. The surface of the pellets were polished by using diamond paste (3, 1, 1/4 μm).

3. TEM/EDS Analysis

3.1. Experimental

To obtain the information of the vicinity of grain boundary, a polycrystalline of $La_{1-x}Ca_xCrO_3$ sintered at $T = 1573\,K$ was crashed by using ion milling technique, and the milled powder was mounted on a copper grid. The lattice images were taken by using the field emission type TEM (JEM-2010F, JEOL, Japan). The accelerating voltage was 200 kV. EDS profiles were collected by using Si(li) SSD type probes (Pentafet, Oxford Instruments). The quantitative analyzes were carried out on each EDS profile with standard-less Cliff-Lorimer ratio thin section method by using TEMQuant® program.

3.2. Results

The lattice image of $La_{0.80}Ca_{0.22}CrO_3$ is shown in Fig. 1(a) The grain boundary which is found at the center of the image is apparently very smooth, and essentially no lattice distortion was observed in the vicinity of grain boundary. The apparent width of the grain boundary is at most 1 nm.

The EDS analyses were made at some spots across the grain boundary, and results are shown as the atomic ratio among calcium, chromium and lanthanum as a function of distance (d) from the grain boundary in Fig. 1(b). The higher calcium concentration and lower lanthanum concentration were found on the grain boundary, $d = 0$. Much more significant calcium enrichment was observed for $La_{0.70}Ca_{0.30}CrO_3$ as shown in Fig. 1(c) This compositional anomaly ceases at the point of 2 nm away from the grain boundary, hence the width of the higher calcium concentration is at most 2 nm around the grain boundary.

(a)

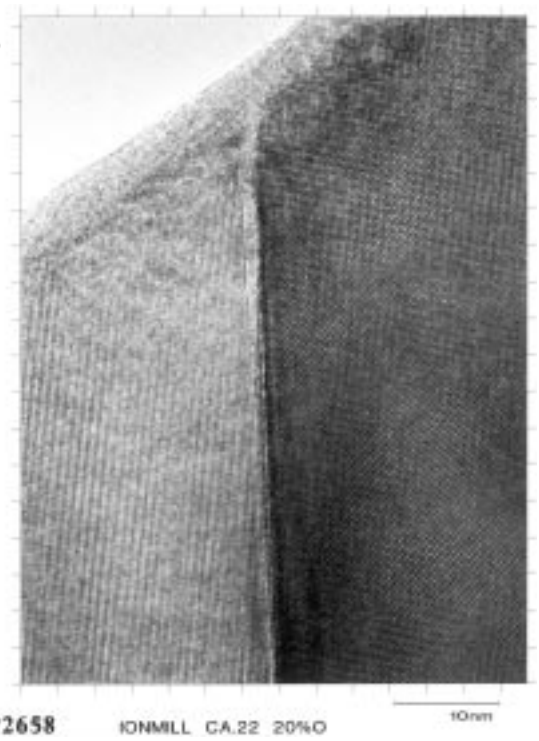

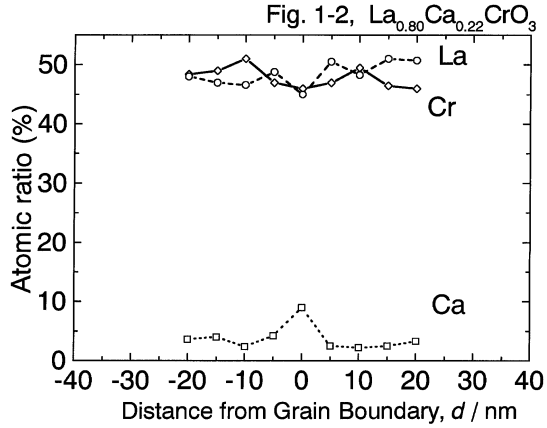

(b)

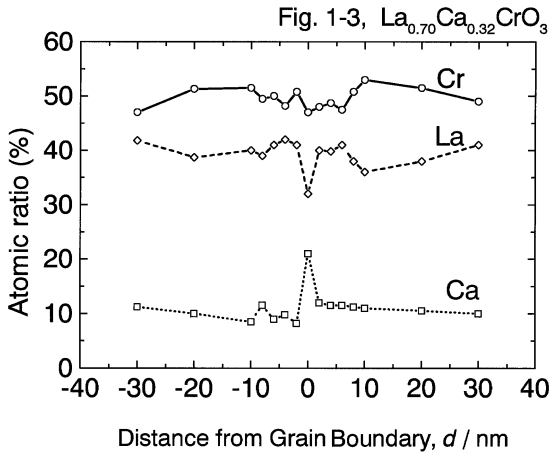

(c)

Fig. 1. TEM image (a), and elemental distribution in the vicinity of a grain boundary of $La_{0.80}Ca_{0.22}CrO_3$ (b) and $La_{0.70}Ca_{0.32}CrO_3$ (c).

4. XPS Analysis on Fractured Surface

4.1. Experimental

XPS profiles were obtained for a fractured surface of $La_{0.70}Ca_{0.32}CrO_3$ by using XL magnet lens mode (ESCALAB 220iXL, VG). Monochromatic X-ray (Al Kα) was used for all measurements. The fractured surface was etched by 2 keV Ar^+ ion sputtering, and several profiles were obtained as a function of sputtering time. The etching rate was estimated by sputtering SiO_2 film on Si substrate as a reference material. The powders of Cr_2O_3, CrO_3, $CaCrO_4$ were also measured as reference materials to determine the valence state of chromium in $La_{0.70}Ca_{0.32}CrO_3$ sample.

4.2. Results

A Cr_{2p} spectrum of an as-fractured surface of $La_{0.70}Ca_{0.32}CrO_3$ is shown in Fig. 2(a). The peak in a higher energy region around $E = 579.7$ eV was assigned to $Cr^{6+}(d^0)$, because the same peak was observed in $CaCrO_4$. The main peak was observed at around $E = 577$ eV with complex broadening which was similar to that of Cr_2O_3. This peak can be deconvoluted by using non linear fitting program to Gauss-Lorenz functions which was developed by Kojima et al. [6], and an example was shown in Fig. 2(a). The background was subtracted by using Shirley's method. The existence of $Cr^{3+}(d^3)$ and $Cr^{4+}(d^2)$ is reasonable because the nominal valence number of chromium in $La_{0.70}Ca_{0.30}CrO_3$ is 3.3 to maintain the charge balance with A-site cations, La^{3+} and Ca^{2+}. However, the existence of Cr^{5+} is questioned, so that these components probably indicates the effect of multiplet term or the charge transfer spectrum of chromium as reported by Howng et al. [7].

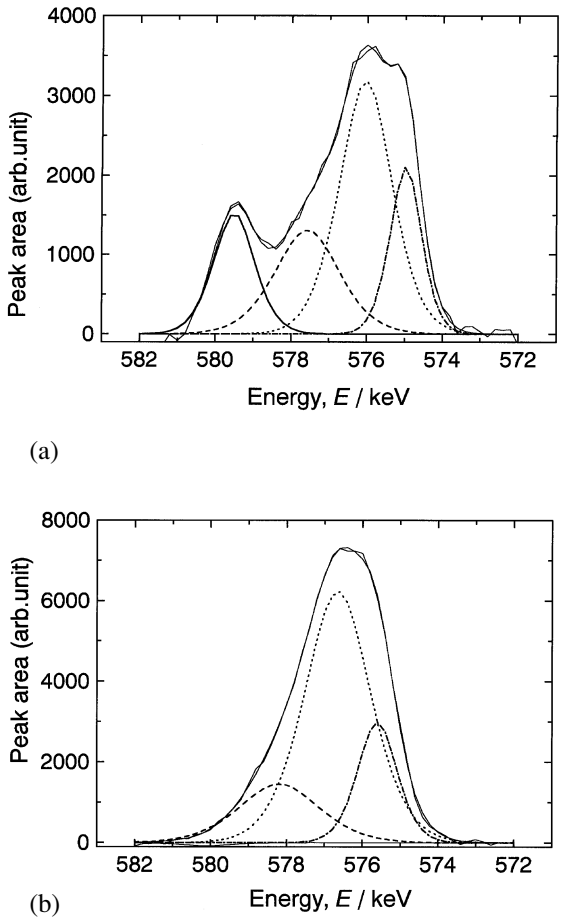

Fig. 2. Intensity of Cr_{2p} peak for as-fractured surface (a) and sputtered surface (b) of $La_{0.70}Ca_{0.32}CrO_3$: ——— raw data The component of different chromium valence states: ——— Cr^{6+}, — — — — Cr^{5+}, - - - - - - Cr^{4+}, — - — - — Cr^{3+}.

The intensity of the high energy peak decreased with Ar^+ sputtering, whereas the intensity of the main peak was kept almost unchanged as shown in Fig. 2(b). The deconvoluted intensities of various valence state of chromium were plotted in Fig. 3 as a functions of etched depth which was calculated assuming the etching rate = 12.5 pm/s. The Cr^{6+} peak was observed only in the vicinity of fracture surface, around 1.2 nm in depth.

5. SIMS Analysis of Interdiffusion of Strontium and Calcium in Sr^{2+}-$La_{0.75}Ca_{0.25}CrO_3$ System

We have tried to determine the interdiffusion coefficient of strontium and calcium in $La_{1-x}Ca_xCrO_3$ by using a simple method, and some

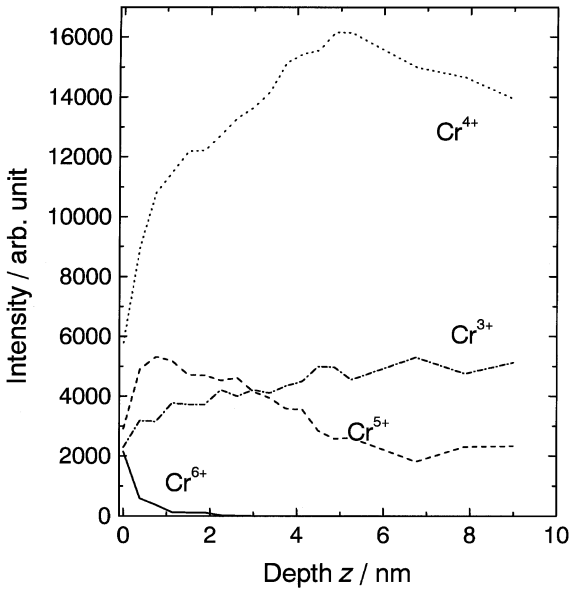

Fig. 3. Chemical states of chromium in the vicinity of grain boundary. Depth (z) mean the distance from the fractured surface.

of the experimental results have already reported elsewhere [8, 9]: A dilute aqueous solution (0.05 N) of $Sr(NO_3)_2$ was painted on the polished surface of $La_{0.90}Ca_{0.11}CrO_3$ or $La_{0.75}Ca_{0.25}CrO_3$ and the samples were annealed at $T = 1173 \sim 1373$ K in $p(O_2) = 10 \sim 10^5$ Pa for $24 \sim 96$ h. The annealed samples were then analyzed by using SIMS (ims5f, CAMECA Instruments) with O_2^+ primary ion (accelerating voltage = 12.5 kV): The depth profile of Ca^+, Cr^+, La^+, and Sr^+ secondary ions on the sample surface were obtained as a function of etching time by the primary ion ($I = 300 \sim 700$ nA). The depth of eroded area was subsequently measured by a surface profiler (Dektak^3, Veeco/Sloan Technology). The interdiffusion coefficients via bulk (D) and via grain boundary (D_{gb}) were calculated by fitting the depth profile to the Fick's second low solved for a semi-infinite media assuming some boundary condition, which is minutely described in elsewhere[8].

The temperature (T) and oxygen partial pressure ($p(O_2)$) dependence of interdiffusion coefficient are shown in Figs 4 and 5, respectively. As shown in Fig. 4, the absolute value and activation energy of present work agrees very well with the results of La^{3+} diffusion in $LaCrO_3$ by Akashi et al. which were determined from the reaction of La_2O_3 and Cr_2O_3 single crystals [10]. The grain boundary diffusion

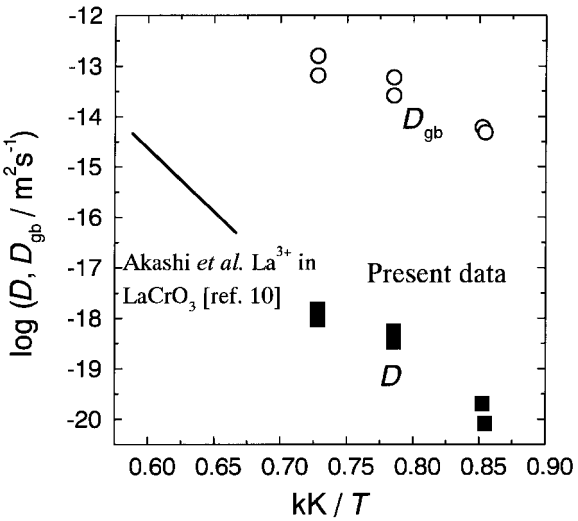

Fig. 4. Temperature dependence of Sr-Ca interdiffusion coefficient via bulk (D) and via grain boundary (D_{gb}) for $La_{0.75}Ca_{0.25}CrO_3$ at $p(O_2) = 10^3$ Pa. The width of grain boundary was assumed to be 1 nm.

coefficients (D_{gb}) were $10^4 \sim 10^5$ times higher than those of bulk, and they seem to have a dependence on $p(O_2)^{0.8}$.

Since the annealed sample was easily fractured along grain boundary, the compositional distribution around grain boundary can be analyzed by obtaining secondary ion images of each cations with a focused primary ion beam ($I < 100$ pA, beam diameter $< 0.3\ \mu$m). Several images were taken by etching the fractured surface, resulting in the three dimensional map of normalized strontium content as shown in Fig.6 [9]. The strontium component has higher concentrations at fractured surface (= grain boundary) and strontium migrated deeply inside the $La_{0.90}Ca_{0.11}\ CrO_3$ polycrystalline. This feature should be compared with the diffusion depth, about a few nm from the fractured surface towards inside polycrystalline.

The width of higher strontium content obtained by present SIMS analyzes was rather large (4 nm) than those obtained in TEM/EDS or XPS analyses. However in this case, we must take into account the atomic mixing effect which was due to the bombardment on the sample surface by focused primary ion with high energy density. Considering the acceleration voltage (12.5 kV) of O_2^+ primary ion, all data shown in Fig. 6. represents the averaged information ca. 10 nm around each measuring spot, which may be the reason why the larger width was obtained.

6. Discussion

6.1. Compositional Distribution and Chromium Valence State at Grain Boundary

The important point to be clarified was how the calcium enrichment is maintained at grain boundaries of $La_{1-x}Ca_xCrO_3$ polycrystalline even after sintering was completed. Although the AES depth profile showed the calcium enrichment at grain boundary, there were many possibilities in the composition of calcium source, for example, CaO, $Ca_m(CrO_4)_n$, $CaCr_2O_4$, or calcium richer $La_{1-x}Ca_xCrO_3$. The present TEM/EDS results indicated that the width of grain boundary was at most 1 nm, and the region of calcium enrichment was only 2 nm from a grain boundary. On the other hand, the width of the Cr^{6+} detectable region in XPS was ca. 1.2 nm, which quantitatively agrees with that of the calcium rich region in TEM/EDS. It means that the calcium enrichment accompanies the oxidation of chromium, and it occurs in a much narrower region than that we previously expected from the data of AES depth profiling (ca. 5 nm). The possibilities of CaO or $CaCr_2O_4$ precipitation are denied because they do not contain any Cr^{6+}. The possibility of the precipitation of $Ca_m(CrO_4)_n$ is also impossible since the width 2 nm corresponds to only a couple of atomic layers, which is too thin to detect the segregation of such a compound. Hence, it is rather reasonable to suppose that the calcium enrichment is established by the formation of calcium rich layer in $La_{1-x}Ca_xCrO_3$ lattice. In the normal perovskite lattice, the higher valence of chromium ions should be accompanied with lowering of the valence number of A-site ions. For this purpose, enrichment of calcium content and the formation of the A-site vacancy can be considered. The former enrichment of calcium is consistent with the present observation by TEM/EDS. In this case, tetravalent Cr^{4+} ions can be present. Since the present XPS results revealed that anomalous high valence state of chromium, Cr^{6+}, was detected, the possibility of A-site vacancy formation should be also considered.

For the chromium ions to be in the hexavalent, the formation of the A-site vacancy is required. Unlike

the WO_3, no perovskite CrO_3 exists in the Cr-O system. Although the significant amount of the A-site vacancies is suggested for the lanthanum manganite, no A-site vacancy formation has been ever suggested for the $LaCrO_3$ except Nb-doped $LaCrO_3$ [11]. This suggests that no A-site vacancy forms in bulk. However, on the surface or in the grain boundary vicinity, the hexavalent chromium (Cr^{6+}) can exist because of the structural incompleteness at grain boundaries. On the surface, the existence of Cr^{6+} has been already suggested by Suvorov et al. [12]

The present TEM/EDS results show very little lattice distortion, which indicates that the ratio of the A-site cations (La^{3+} and Ca^{2+}) to Cr^{6+} does not change across the grain boundary. This suggests that the A-site vacancies are found only on the grain boundaries. In other words, the presence of Cr^{6+} at grain boundaries may cause an additional change in the structure, which is normally expected due to the irregularity of the ionic configuration.

6.2. *Role of Grain Boundary on Fast Material Transport in* $La_{1-x}Ca_xCrO_3$

The presently obtained Sr-Ca interdiffusion coefficients reveal that the grain boundary diffusion coefficients, D_{gb}, was much faster than those of bulk D, so that fast material transport in Sr^{2+}-$La_{1-x}Ca_xCrO_3$ is mainly governed by grain boundary diffusion. Since logarithm of D_{gb} linearly increases with logarithm of oxygen partial pressure $p(O_2)$, some reduction/oxidation reactions are considered to play important roles in diffusion process.

The presently observed TEM/EDS and XPS results show the presence of hexavalent chromium in the vicinity of thin grain boundary and no lattice distortion, which suggest the presence of A-site vacancy in perovskite lattice. According to the Kröger-Vink notation, the formation reaction can be expressed as follows:

$$Ca'_{La} + Cr^{\bullet}_{Cr} + \frac{1}{2}O_2 \leftrightarrow V'''_{La} + Cr^{\bullet\bullet\bullet\bullet}_{Cr} + CaO \qquad (1)$$

$$K = \frac{[V'''_{La}][Cr^{\bullet\bullet\bullet\bullet}_{Cr}][CaO]}{[Ca'_{La}][Cr^{\bullet}_{Cr}]p(O_2)^{\frac{1}{2}}} \qquad (2)$$

where Ca'_{La} is a Ca^{2+} ion at A-site (lanthanum site), $Cr^{\bullet}_{Cr}$ is a Cr^{4+} ion at B-site (chromium site), $Cr^{\bullet\bullet\bullet\bullet}_{Cr}$ is a Cr^{6+} ion at B-site, V'''_{La} is an A-site vacancy, and K is the equilibrium constant.

Most of the atoms in the vicinity of grain boundary are thought to be not so mobile as atoms in liquid phase, although the grain boundary has much more structural incompleteness than in bulk. Therefore it is reasonable that the strontium diffusion at grain boundary is made by a similar mechanism as that in bulk, that is, cation exchange of Ca^{2+} and Sr^{2+} at A-sites in perovskite lattice, in which the A-site vacancy plays a very important role. The activation energy of between grain boundary diffusion coefficient is 217 kJ/mol[9], and this value is almost the same as the activation energy of bulk diffusion coefficient (258 kJ/mol), which may support the assumption of the same diffusion mechanism. As shown in Eq. (1), the formation of A-site vacancy inevitably accompanies the oxidation of chromium, or in other words, the formation of Cr^{6+}. Thus the A-site vacancy concentration at the grain boundary is probably much higher than that in the bulk, which greatly affects on the diffusion coefficient at grain boundary.

Although we confirmed the existence of Cr^{6+} at room temperature XPS, there was no proof for the existence of Cr^{6+} at higher temperatures. There still remained the possibility that the hexavalent chromium might form in cooling procedure, because the oxide ions also diffuse as fast as that of cations at grain boundaries [13]. However, the $p(O_2)$ dependence of Sr-Ca interdiffusion coefficient at grain boundary indicates that the hexavalent chromium indeed exists at annealing temperatures in diffusion experiment, because the concentration of $Cr^{\bullet\bullet\bullet\bullet}_{Cr}$ directly depends on $p(O_2)^{0.5}$ as derived from Eq. (2).

The derived $p(O_2)$ dependence of diffusion coefficient should be compared with the experimental results, which apparently showed the linear dependence on $p(O_2)^{0.8}$ as shown in Fig. 5. Although the $p(O_2)^{0.5}$ dependence is expected when the oxidation from Cr^{4+} to Cr^{6+} is assumed as above, the experimental results indicate the possibility of more drastic of valence changes, for example from Cr^{3+} to $Cr^{6+}(p(O_2)^{0.75})$, or even more. The actual chemical state at grain boundary is of course much more complicated than that expected in the discussion above. In view of this correlation, the diffusivity of chromium ions themselves becomes of great interest. It is hoped to measure the diffusion coefficient of chromium along the grain boundaries and to compare with those of calcium ions and oxide ions.

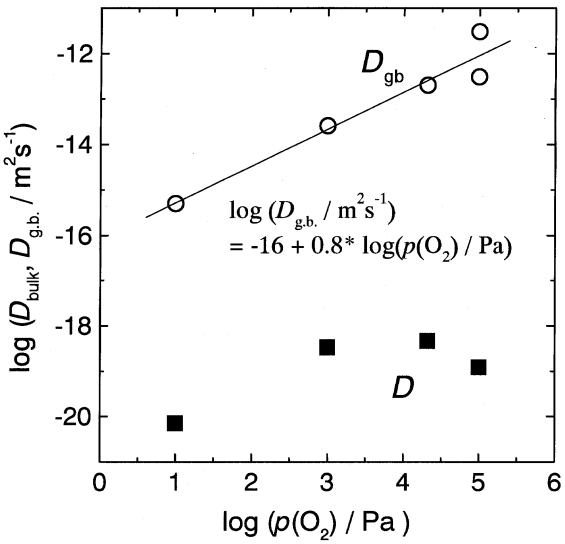

Fig. 5. Oxygen partial pressure dependence of Sr-Ca interdiffusion coefficient via bulk (D) and via grain boundary (D_{gb}) for Sr^{2+}-$La_{0.75}Ca_{0.25}CrO_3$ at $T = 1273$ K.

6.3. *Comparison with Bulk Properties*

The present results clarified that at grain boundaries, Cr^{6+} ions are present and that makes diffusion along grain boundaries extremely fast. This is consistent with the fact that this material was sintered rapidly by liquid sintering mechanism. It is suggested that the present grain boundaries are quite similar to the liquids appearing as bulk substances. In the La-Ca-Cr-O system, the liquid phase appearing around $T = 1273$ K shows the following properties [3];

(a) calcium is rich
(b) high chromium valence state
(c) mass transport is fast enough to assist the sintering

These features are common to those at the grain boundaries which have been determined in the present study. Since the present TEM/EDS does not indicate any liquid nor amorphous phases at grain boundaries, the above similarity can be interpreted that thermodynamically as follows:

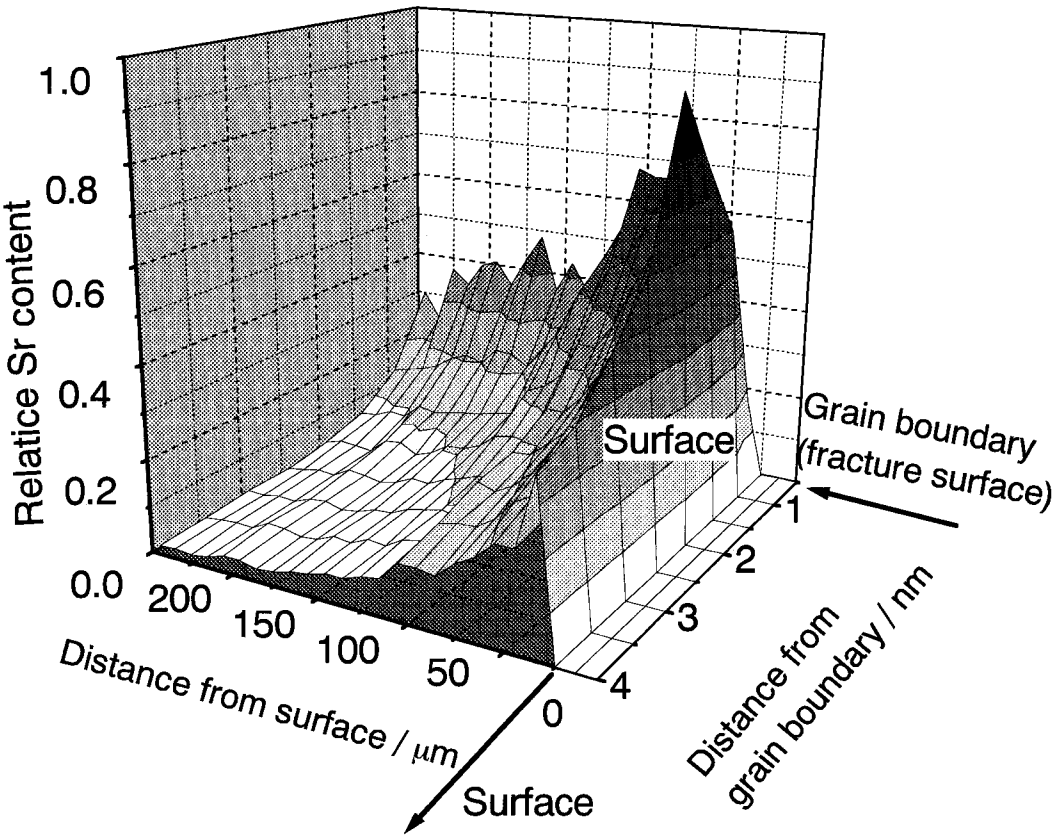

Fig. 6. Three-dimensional map of normalized strontium content around the fractured surface (= grain boundary) of Sr^{2+}-$La_{0.90}Ca_{0.11}CrO_3$[9]. Annealing condition: $T = 1273$ K, $p(O_2) = 21$ kPa (in air), $t = 72$ h.

1. The common feature among liquids and grain boundaries is that the structure is no longer regular. In the thermodynamic terms, this corresponds to the large molar entropy and large molar volume.
2. When we assume the local equilibrium across the grain boundary, the molar Gibb's energy (in other words, chemical potential) should be constant. Since the molar entropy is large at grain boundary, the molar enthalpy should be also large according to the second law, $g(=\mu) = h - sT$.
3. In view of the above consideration, the temperature dependence of grain boundary properties is quite interest. In bulk substance, the entropy change between liquid and solid are very large, therefore, the stable region of liquid is limited only at high temperatures. At grain boundaries, the mobility of most atoms is not so affected by temperature so that the entropy difference is not large. Still, some difference is expected from the structural differences. In view of this, it is of interest to examine the temperature dependence of grain boundary properties. At present, the temperature dependence of Sr-Ca interdiffusion coefficient is available as given in Fig. 5. From this behavior, it is hard to find any difference between bulk and grain boundary. Since the clear difference was detected between bulk and grain boundary in the oxygen potential dependence described above, it is hoped to clarify the differences in the temperature dependence in cation and oxide ion diffusion coefficient.

7. Conclusion

The present TEM and XPS results made it possible to correlate the microscopic compositional distribution with the macroscopic materials transport phenomena: The width of grain boundary of $La_{1-x}Ca_xCrO_3$ polycrystalline is at most 1 nm and the calcium enrichment and higher chromium valence state was observed in the range of 2 nm from a grain boundary. This compositional change is supposed to be mainly due to the enrichment of Ca in the A-site of perovskite lattice. The fast interdiffusion of strontium and calcium in $La_{1-x}Ca_xCrO_3$ is thought to be governed by cation exchange in perovskite lattice, where A-site vacancies can be introduced by the oxidation of chromium.

References

1. N. Q. Minh, *J. Am. Ceram. Soc*., **76**(3), 563 (1993).
2. N. Sakai, T. Kawada, H. Yokokawa, M. Dokiya, and T. Iwata, *Solid State Ionics*, **40/41**, 394 (1990).
3. N. Sakai, T. Kawada, H. Yokokawa, and M. Dokiya, *J. Am. Ceram. Soc*., **76**(3), 609 (1993).
4. N. Sakai, T. Kawada, H. Yokokawa, and M. Dokiya, in *Science and Technology of Zirconia V*, ed. by S.P.S. Badwal, M.J. Bannister, and H.J. Hannink (Technomic Publishing Co. Ltd., Lancaster, PA, USA, 1993), p. 764.
5. M. P. Pechini, U.S. Patent No. 3,330,697 (1967).
6. I. Kojima and M. Kurahashi, *J. Elec. Spectr. Relat. Phenom.*, **42**, 177 (1987).
7. W. Y. Howng and R. J. Thorn, *J. Phys. Chem. Solids*, **41**, 75 (1980).
8. T. Horita, N. Sakai, H. Yokokawa, M. Dokiya, and T. Kawada, *J. Am. Ceram. Soc*., **81**(2), 315 (1998).
9. N. Sakai, K. Yamaji, T. Horita, M. Ishikawa, H. Yokokawa, and M. Dokiya, in *Solid Oxide Fuel Cell V*, ed. by U. Stimming, S. C. Singhal, H. Tagawa, and W. Lehnart, *The Electrochem. Soc. Proceedings*, Volume **97-40**, (The Electrochem. Soc., Pennington, NJ, USA, 1997), p. 1283.
10. T. Akashi, M. Nanko, T. Maruyama, Y. Shiraishi, and J. Tanabe, *ibid*., pp. 1263 (1997).
11. C. J. Yu, H. U. Anderson, and D. M. Sparlin, *J. Solid State Chem.*, **78**, 242 (1989).
12. S. A. Suvorov, V. P. Migal, and V. V. Gusanov, *Zh. Prikal. Khimi*, **61**(18), 1910 (1988).
13. N. Sakai, T. Horita, H. Yokokawa, M. Dokiya and T. Kawada, *Solid State Ionics*, **86-88**, 1273 (1996).
14. J. Mizusaki, S. Yamauchi, K. Fueki, and A. Ishikawa, *Solid State Ionics*, **12**, 119 (1984).